CEBAF Program Advisory Committee Six (PAC6) Proposal Cover Sheet

This proposal must be received by close of business on April 5, 1993 at:

CEBAF
User Liaison Office
12000 Jefferson Avenue
Newport News, VA 23606

Proposal Title

THE CHARGE FORM FACTOR OF THE NEUTRON

Contact Person

Name: DONAL DAY
Institution: UNIVERSITY OF VIRGINIA
Address: DEPARTMENT OF PHYSICS
Address: JESSE BEAMS LAB
City, State ZIP/Country: CHARLOTTESVILLE, VA 22901
Phone: 804 - 924 - 6566 **FAX:** 804 - 924 - 4576
E-Mail → BITnet: DONAL@ATHENA.PHYS.VIRGINIA.EDU **Internet:**

If this proposal is based on a previously submitted proposal or letter-of-intent, give the number, title and date:

89-018
THE ELECTRIC FORM FACTOR OF THE NEUTRON FROM THE ^{2}H(e,e'n)p

CEBAF Use Only

Receipt Date: 4/5/93 Log Number Assigned: PR 93-026

By:

CEBAF PROPOSAL
The Charge Form Factor of the Neutron

D. Crabb, C. Cothran, D. Day (Spokesperson), S. Høibråten
R. Lindgren, R. Lourie, J. S. McCarthy, P. McKee, R. Minehart,
D. Počanić, O. Rondon-Aramayo, R. Sealock, C. Smith, and A. Tobias
Institute of Nuclear and Particle Physics
Department of Physics, University of Virginia
Charlottesville, VA 22901, USA

A. Feltham, D. Fritschi, J. Jourdan, M. Loppacher,
G. Masson, S. Robinson, I. Sick and P. Trueb
Institut für Physik, Universität Basel,
CH-4056, Basel, Schweiz

R. Carlini, D. Mack, J. Mitchell, C. Sinclair,
B. Vulcan, S. Wood, and C. Yan
Continous Electron Beam Accelerator Facility
Newport News, VA, 23606

April 5, 1993

Contents

1 Introduction

The form factors of the proton and neutron give information on fundamental properties of the nucleon, and provide a critical testing ground for models based on QCD. A detailed knowledge of these quantities is also essential to our understanding of the electromagnetic response functions of nuclei.

Our present knowledge of the neutron electric form factor is inadequate. The slope of $G_{en}(Q^2)$ at $q^2 = 0$ is accurately known from neutron-electron scattering. At higher Q^2 systematic errors are very large. There, G_{en} has been extracted from elastic $e-d$ scattering, or inclusive quasielastic $e-d$ scattering. In both cases removal of the proton contribution requires information about the deuteron structure and large uncertainties are introduced. Uncertainties in the theoretical description of the deuteron (mostly from FSI and MEC contributions) have especially negative consequences. As a result, G_{en}, until very recently, was known with a systematic error of about $\pm$ 100 % . A new experiment at Saclay [1] on $e-d$ elastic scattering has improved the situation at $Q^2 < 0.8$; the resulting systematic errors are $\simeq$ 30%. Serious doubts remain as a great deal of theoretical input on non-relativistic deuteron structure, relativistic effects and MEC are needed to infer G_{en} from elastic $e-d$ data. Figure 1 shows the best fits to the inferred G_{en} obtained by different models for the N-N interaction necessary to compute the deuteron structure. Such uncertainties and ambiguities are unsatisfactory for a quantity as fundamental as G_{en}. With the experiment proposed here we will be able to determine G_{en} without large theoretical corrections.

The large systematic errors in the past experiments result from two difficulties.

- For elastic e-d scattering the deuteron structure is very important: Accounting for it introduces errors which are magnified with the subsequent subtraction of the dominant proton contribution.

- For quasielastic e-d scattering, the longitudinal/transverse Rosenbluth separation introduces large systematic errors for the small term (charge). Furthermore the necessary subtraction of the dominant proton contribution increases the large systematic errors.

To improve this situation we need to study a reaction which is insensitive to the deuteron structure, which avoids a subtraction of the proton contribution and which avoids longitudinal/transverse Rosenbluth separation.

In this proposal we describe in detail an alternative way of extracting the Sachs Coulomb form factor G_{en}, by measuring the spin-dependent part of the elastic $e-n$ cross section. To this effect, we plan to detect quasielastically scattered electrons from a longitudinally polarized beam incident on polarized deuterium nuclei in deuterated ammonia (ND_3). The determination of the asymmetry in the cross section for two opposite orientations of either polarization, yields the product $G_{en} \cdot G_{mn}$. In the remainder of the proposal we will review the exact relation between G_{en} and

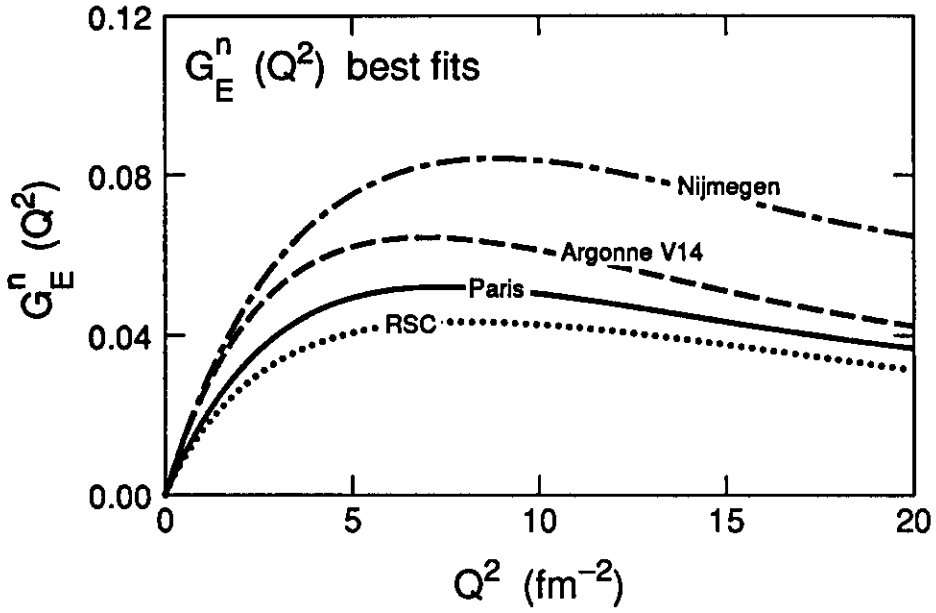

Figure 1: Two parameter fits to data for G_{en} deduced from the $d(e,e)$ data using deuteron wave functions calculated with the Paris (solid), RSC (dotted), Argonne V14 (dashed) and Nijmegen (dash-dotted) potentials. From Reference [1].

the experimental asymmetry, explore the kinematic region where the method may be applied, and discuss the technical details of the polarized target, the electron and the neutron detector systems, polarimeter and the auxiliary devices involved. An analysis of the estimated uncertainties as well as the count rates and beam time request complete the proposal.

2 Proposed technique

Dombey[2] was the first to point out that the scattering of longitudinally polarized leptons on polarized nucleon targets could be used to determine the form factors of the nucleons. The procedure consists of measuring the part of the $e-N$ elastic cross section that corresponds to the interference between the Coulomb and the transverse components of the nucleon current. The interference term is extracted from a measurement of the asymmetry in the cross section when the beam or the target polarization is reversed.

Following Donnelly and Raskin[3, 4] we can express the inclusive $e-N$ cross section as a sum of an unpolarized part (Σ), that corresponds to the elastic cross section $d\sigma/d\Omega_e$, and a polarized part (Δ), that is different from zero only when the

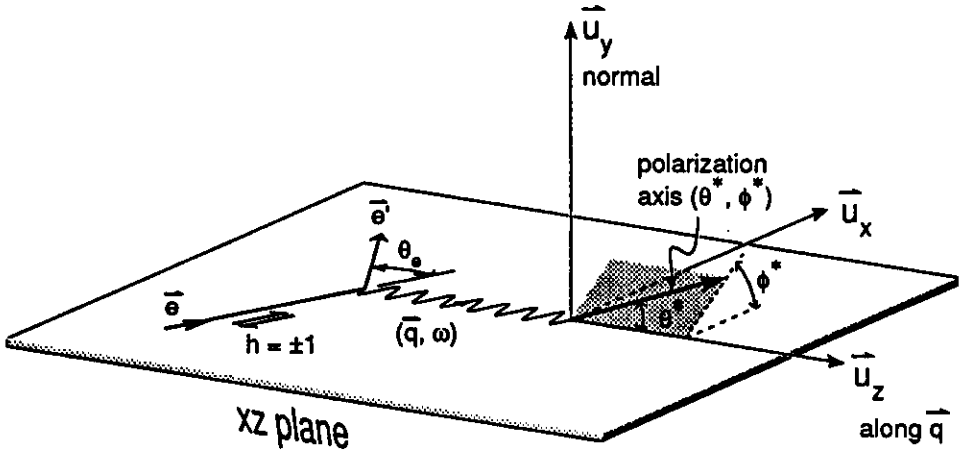

Figure 2: Coordinate system for $\vec{p}(\vec{e}, e')$ with orientation of polarization axis shown.

beam is longitudinally polarized (helicity h): [1]

$$\sigma(h) = \Sigma + h\Delta; \quad h = \pm p_{beam}. \tag{1}$$

The asymmetry is then

$$A_n = \frac{\sigma_+ - \sigma_-}{\sigma_+ + \sigma_-} = \frac{\Delta}{\Sigma}. \tag{2}$$

As stated above, Σ is just the elastic unpolarized free $e - N$ cross section, and specifically for neutrons it reads

$$\Sigma = \sigma_{Mott}\frac{E'}{E_0}\Big(\frac{G_{en}^2 + \tau G_{mn}^2}{(1+\tau)} + 2\tau G_{mn}^2 \tan^2(\theta_e/2)\Big), \tag{3}$$

where $E_0(E')$ is the electron's initial (final) energy, $\tau = Q^2/4m_n^2$, m_n is the neutron mass, $-Q^2 = q_\mu^2$ is the square of the four- momentum transfer and $G_{e,mn}$ are the neutron Coulomb and magnetic form factors. The polarized part Δ contains two terms, associated with the possible directions of the target polarization. The full expression is given below, with the kinematic factors and the nucleon form factors both evaluated in the laboratory frame (the elastic recoil factor f_{rec}^{-1} reduces to E'/E_0 in the extreme relativistic limit):

$$\begin{aligned}\Delta &= -2\sigma_{Mott}\frac{E'}{E_0}\sqrt{\frac{\tau}{1+\tau}}\tan(\theta_e/2) \\ &\quad \cdot\Big\{\sqrt{\tau(1+(1+\tau)\tan^2(\theta_e/2))}\cos\theta^* G_{mn}^2 + \sin\theta^*\cos\phi^* G_{en}G_{mn}\Big\}\end{aligned} \tag{4}$$

where θ^* and ϕ^* are the laboratory angles of the target polarization vector with $\vec{q}$ along the $\vec{u}_z$ direction and $\vec{u}_y$ normal to the electron scattering plane. It is clear

[1]The longitudinal beam helicity is defined as parallel or opposite the beam momentum. See Figure 2 for the definition of the reference frame.

that to extract G_{en} the target has to be polarized longitudinally (i.e. $\phi^* = 0$) and perpendicular to $\vec{q}$ ($\theta^* = \pi/2$). For this special condition, the asymmetry simplifies to

$$A_n = \frac{\Delta}{\Sigma} = \frac{-2\sqrt{\tau(1+\tau)}\tan(\theta_e/2)G_{en}G_{mn}}{G_{en}^2 + \tau(1+2(1+\tau)\tan^2(\theta_e/2))G_{mn}^2}. \quad (5)$$

This result was also obtained by Arnold *et al.*[5] who considered the measurement of the polarization of the recoil neutron, instead of using a polarized target.

The foregoing analysis is valid for free nucleons, and it has been reinterpreted in the case of neutrons in polarized nuclei. For the specific case of polarized deuterium nuclei, the exclusive process involving the detection of the neutron after the electrodisintegration can be similarly described[3] in an expression where the interference between G_{en} and G_{mn} is contained in the polarized part.

The neutron asymmetry is related to the deuteron asymmetry A_{eD}^v, as $A_n = \gamma^{-1}A_{ed}^v$ where γ is a correction factor (0.92) for the D–state of the deuteron.

There are different ways to exploit polarization observables for a determination of $G_e \cdot G_m$. One can either use a polarized beam and target as discussed above, or one can use a polarized beam and measure the polarization of the recoiling nucleon. In practice, the measurement using a polarized beam and target involves determining the experimental asymmetry

$$\epsilon = \frac{N_+ - N_-}{N_+ + N_-} = p_{beam}P_d^1 A_{ed}^V, \quad (6)$$

which depends on the normalized numbers of counts for two opposite helicities, N_+ and N_-. The same expression occurs in the recoil polarimetry method, with the obvious reinterpretation of P_d^1 as the analyzing power of the polarimeter, A_x; A_{ed}^V is then the polarization P_x' of the recoiling nucleon, and $N_\pm$ are the numbers of counts in the up(down) segments of the polarimeter.

Our studies of these alternatives have led us to choose the polarized target technique. We have found that it allows us to measure $G_e n$ over a larger range of Q^2 than the alternative, and it avoids the difficult problem of a new calibration of the recoil polarimeter for every neutron energy (for every Q^2). In addition, the same setup (target and detectors) can be used to check the experimental technique and the reaction mechanism, assumed to be quasi-free knockout , by measuring G_{ep} which is known over the Q^2 range we wish to study.

There are two different polarized targets which provide in effect polarized neutrons, polarized deuteron and polarized ^{3}He. We have chosen polarized deuteron, as the theoretical description of the $(e, e'n)$ process is on a much firmer footing. For the 2N-system the final state interaction can be treated exactly, while this is questionable for $A = 3$. The role of the D-state in the ground state wave function and the contributions of MEC, are under better control. Accurate calculations are already available, while for A = 3 we are still speculating on the size of the effects. At the same time, a deuteron target allows the experimental check on procedures

and reaction mechanism through the comparison of the $d(e,e'n)$ and $d(e,e'p)$ reactions. Arenhövel *et al.*[5] have shown that, for the case of the deuteron, the uncertainties introduced by the deuteron structure are very small if one concentrates on the strength corresponding to quasielastic $e-n$ scattering with neutrons of small initial momentum. For such kinematic conditions and for the special case of the two-nucleon system, FSI can be accurately computed, and does not contribute significantly to the systematic errors. The effects of MEC, which for A = 2, also can be calculated with reasonable confidence, are small as well. Effects of both FSI and MEC are much smaller than the statistical and systematical errors of the experiment we propose.

To determine the region of Q^2 where the proposed technique may be most effective, the evaluation of a figure of merit (FOM) has become customary. In the present case, the figure of merit is related to the time required to accumulate the number of counts needed to determine the asymmetry to a given precision. This number is proportional to the product of the square of the asymmetry times the cross section (averaged over the acceptances of our detectors), so the FOM is defined as

$$FOM = A_n^2 \frac{d\sigma^3}{d\Omega_e d\Omega_n dE'}.$$

Obviously, this quantity depends on the choice of a model for G_{en}.

Several models have been tried to describe the existing data, which extend from the photon point to $Q^2 \cong 0.8(\mathrm{GeV/c})^2$. Among those deserving special attention are the so-called "dipole" model which uses the form $G_{en} = -\tau G_{mn} = -\tau \mu_n G_{ep}$, with $G_{ep} = (1+Q^2/0.71)^{-2}$, in fact setting the Dirac form factor F_{1n} to zero, in the full expression for the Sachs form factor $G_{en} = F_{1n} - \tau F_{2n}$; the phenomenological parameterization of Galster *et al.*[7], $G_{en} = -\tau G_{mn}/(1+p\tau)$; and the models that seek a connection between the value of of the form factors at low momentum transfer and the asymptotic values of the Dirac and Pauli form factors F_{1n} and F_{2n} predicted by perturbative QCD, in particular the one proposed by Gari and Krümpelmann[8].

In Figure 3 we present the Q^2 dependence of G_{en} in those three instances. It can be seen that the dipole model is higher than the two others, and in fact it is an upper bound to the experimental data. On the other hand, the Galster parameterization (with the Feshbach-Lomon potential) gives a good fit for p = 5.6. We used these two models, which cover a broad range of possible values for the Q^2 dependence of G_{en}, to compute the FOM's. These studies show that the scattered electron angle θ_e should be small, as the FOM has a maximum (although a very flat one) at small angles.

For increasing momentum transfer, the FOM drops by a factor of $\sim$ 100 (depending on the model) from its maximum value to the largest momentum transfer considered here, $Q^2 = 2(\mathrm{GeV/c})^2$. This places a practical limit on the upper value of the attainable momentum transfer, independent of other technical complications that arise from the high kinetic energy of the recoil neutrons, and the opening of inelastic $(e,e'\pi)$ and $(n,p\pi)$ channels. Therefore, in the present experiment, we will

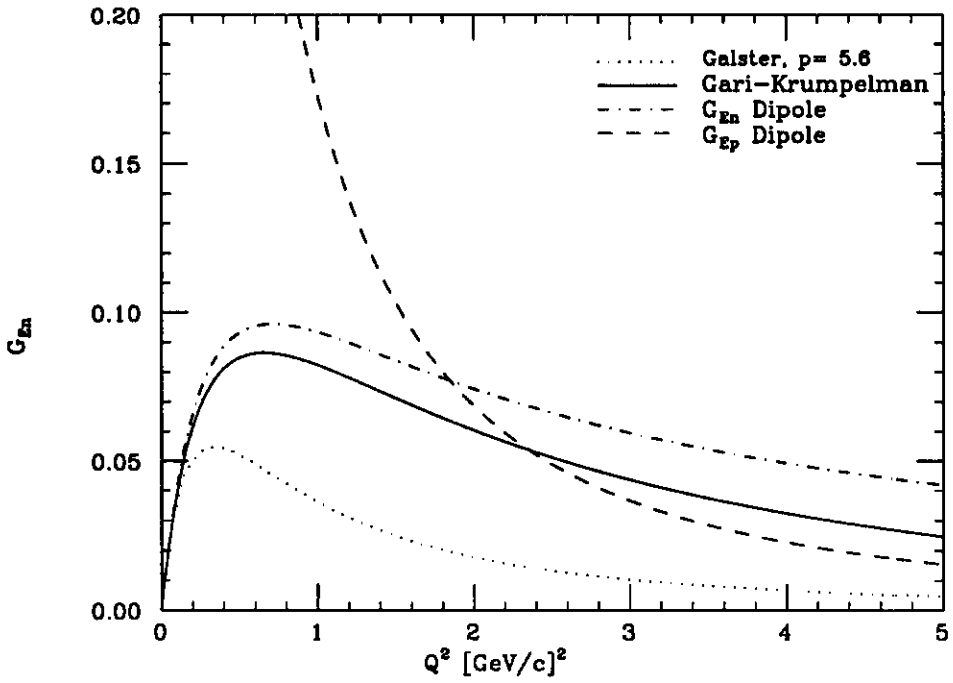

Figure 3: Q^2 dependence of G_{en} for three different models.

Q^2 $(GeV/c)^2$	E_0 GeV	θ_e	ν_{qe} GeV	q GeV/c	θ_q	θ_B	T'_n MeV
0.50	2.85	15.00°	0.269	0.757	62.05°	27.95°	267
1.00	3.97	15.56°	0.534	1.134	54.41°	35.59°	533
1.50	3.97	19.87°	0.800	1.463	47.45°	42.53°	799
2.00	3.97	24.03°	1.067	1.771	41.92°	48.08°	1065

Table 1: Kinematical quantities

attempt to extract G_{en} at four values of Q^2, starting at about 0.5 $(GeV/c)^2$, up to 2 $(GeV/c)^2$.

To obtain these values of the four-momentum transfer, a combination of beam energies and scattering angles are chosen such as to maximize the FOM, within the laboratory capabilities and facilities. The kinematical settings we have chosen are displayed in table 1.

The symbols in this table have been defined earlier, with the exception of ν_{qe}

which is the electron energy loss at the quasielastic peak, including the average separation energy of the nucleon; θ_B which is the direction of the target magnetic field relative to the beam in the laboratory reference frame (main coordinate system), and is perpendicular to $\vec{q}$, corresponding to the values $\theta^* = \pi/2, \phi^* = 0$; and T'_n is the kinetic energy of the recoil neutrons in parallel kinematics (i.e. zero initial momentum).

The theoretical studies performed indicate clearly that $\vec{d}(\vec{e}, e'n)p$ will provide a clean determination of G_{en} with small systematic errors. This is an important criterion given the fact that past attempts to measure G_{en} were all limited by systematic errors in both experiment and, even more so, in the theoretical input necessary to infer G_{en}.

3 Polarized Target

The schematic of the polarized target assembly is shown in Fig. 4. It consists of a superconducting dipole which operates at 5 Tesla and the target refrigerator which operates at a temperature of 1K. The magnet is a split Helmholtz coil which produces a longitudinal field. A bore of 20 cm and an opening angle of 100 degrees together with a coil split of 8 cm and a 34 degree opening angle between the coils allow for great flexibility in field orientation and particle detection.

Figure 4 also shows the ^{4}He evaporation refrigerator necessary to cool the target to a temperature of 1K. Such a refrigerator is the best choice for the beam conditions of this experiment in which efficient heat removal is required. Large pumps mean that operation close to 1K, and therefore high polarizations, is possible. Using the pumps on hand, 1.5 W of heat can be removed.

The target material is doped, by irradiation or chemical means, with paramagnetic centers (unpaired electrons) which at 1K and 5T will be nearly 100% polarized. Irradiation with microwaves (140 GHz at 5T) transfers most of the electron polarization to the protons in the material. The transfer mechanism is less effective with deuterons. By this method of dynamic nuclear polarization [14] protons have been polarized to almost 100% and deuterons to 50%. The material of choice for this experiment is ammonia, NH_3 and ND_3.

In experiments with ionizing particles, radiation damage to the material causes the polarization to fall. The polarization, P, after an incident flux, I, is given by: $P = P_{init}e^{-I/I_0}$. For most materials $I_0 = 10^{14}$ particles/cm^2 [15]. For ammonia $I_0 > 10^{15}$ particles/cm^2[16].

The polarization can be largely recovered by annealing, i.e. warming the target to a characteristic temperature, usually around 100K. But in most materials there is a residual, non-annealable radiation damage component. This means that the target material must be changed after a few anneals (~ 10) because the achievable polarization falls to an unacceptably low level. Ammonia, however, can be repeatedly annealed and the polarization completely recovered.

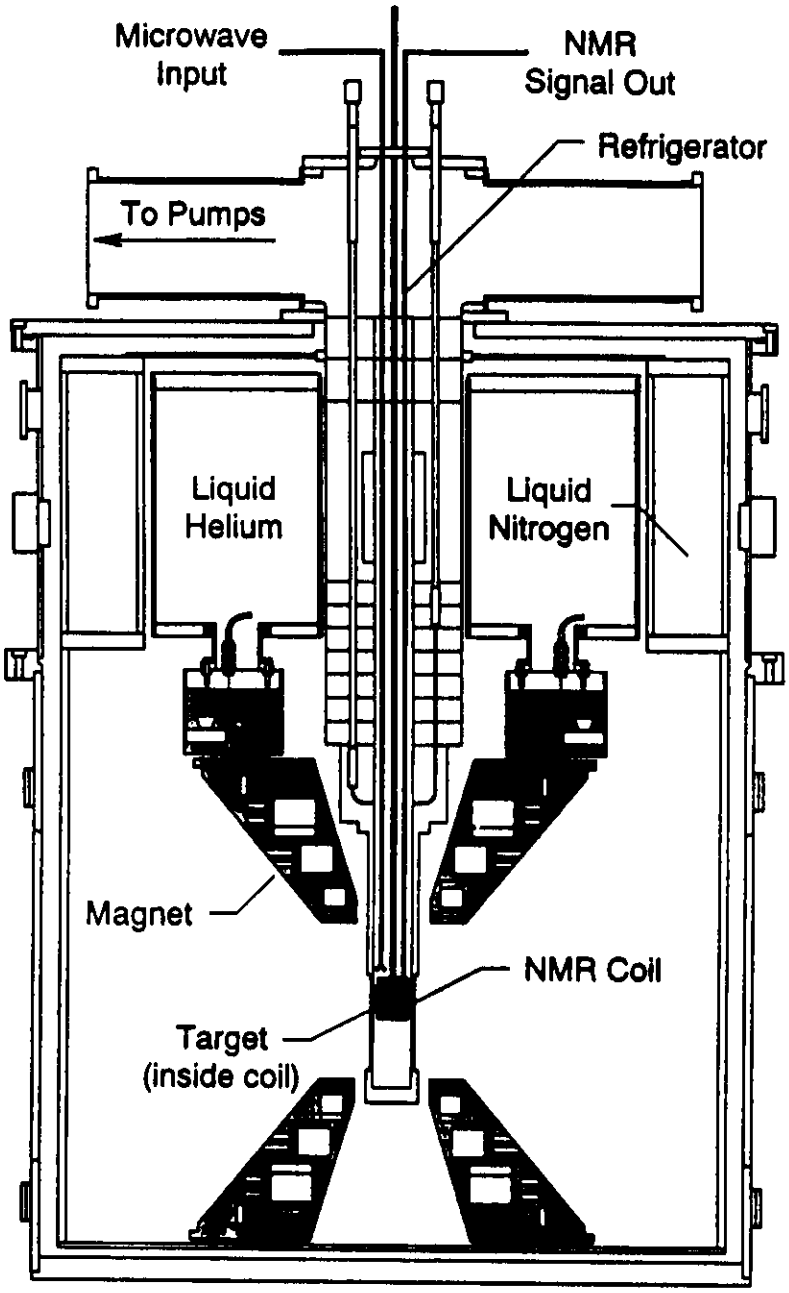

Figure 4: Cross section view of the polarized target

The paramagnetic doping for ammonia must be done by irradiation rather than the more usual chemical methods. The simplest method is to irradiate the ammonia in its frozen state, under liquid argon, with a low energy electron beam (20 - 300 MeV), but other methods have been used. The best results have been obtained with $10^{16} - 10^{17}$ e^-/cm^2 incident on the target [16, 17]. However it has been observed that

'in situ' irradiation [16, 17] enhances the polarizability of the ammonia, particularly in the case of ND_3.

In order to spread the beam over the target to get uniform heat deposition, the Hall C rastering system is being designed [22] to allow the beam to be rastered over the full area of the target, 2cm · 2cm. The large excursions from the nominal beam axis require in particular, that the angle change produced by the upstream rastering system is compensated near the target with a second rastering magnet, such that the beam continues after the target to the beam dump.

The polarized assembly for this experiment was set up at the University of Virginia and became completely operational in August 1992. It was operated through February 1993 with many target material investigations being carried out. All subsystems and components were tested over this period. The magnet and refrigerator were kept cold, at 4K and 10K respectively, so that the magnet could be ramped up on demand and at the same time the refrigerator could be made to operate at 1K. It took 45 minutes for the magnet to reach 5T and polarization tests could be started immediately afterwards.

At UVA, protons in NH_3 were polarized to 95%, while the deuterons in ND_3 reached 13% polarization, using ammonia irradiated at the Saskatoon Accelerator Lab. Subsequent irradiations at CEBAF have indicated that the deuteron polarization is very sensitive to the number of paramagnetic centers produced, i.e. dose. Work is continuing to find the optimum dose, and then with further 'in situ' irradiation a deuteron polarization of 40 - 45% is expected. We base these expectations on work done with the Yale target at SLAC some 15 years ago, where they reached a deuteron polarization of 27% despite having modest cooling power and reaching only 75% for the polarization of NH_3. The polarized target work at Bonn in 1985 achieved 30% deuteron polarization at 2.5 T, with only 70% polarization for NH_3. In a different configuration the Bonn group actually did achieve 45% polarization for ND_3.

Two microwave tubes were tested, both EIOs, one operating at 140 GHz, the other at 136 GHz. Each tube was used to polarize ammonia and delivered up to 500 mW to the target volume. The NMR system was developed to work with both a signal generator and a frequency synthesizer. The critical performance level was the observation and measurement of the deuteron thermal equilibrium signal. We have achieved a signal of similar quality to that achieved in the SMC experiment at CERN [21] although in our case there was no temperature stabilization of the critical components. This stabilization will be incorporated in future set-ups. In March 1993 everything was dismantled and shipped to SLAC for experiment E143.

At SLAC, as for this G_{en}experiment, ammonia with ^{15}N will be the target material of choice. Because the nitrogen is also polarized, $^{15}NH_3$ and $^{15}ND_3$ are preferred since the polarization of the ^{15}N is carried by the proton rather than the proton *and* the neutron as in the case of ^{14}N. The degree of polarization is the same in either case but much easier to measure for ^{15}N. It has also been shown [18] that the radiation performance is the same for ^{14}N and ^{15}N ammonia.

Detail	NH_3	ND_3
Target Length	2.5 cm	2.5 cm
Temperature	1.0 K	1.0 K
Current	100 nA	40 nA
Luminosity (N/cm^2,s)	$1 \cdot 10^{35}$	$4 \cdot 10^{34}$
Vector Polarization	0.9	0.4
Tensor Polarization		0.12

Table 2: Expected target performance

With the absence of a polarized neutron background from $^{15}ND_3$, the systematic error will be substantially reduced in the measurement of G_{en}. $^{15}NH_3$ and $^{15}ND_3$ will be loaded into two separate target containers in the refrigerator and a simple mechanism will put either target into the beam on demand.

The operation of the target at SLAC will set the performance standard for operation at CEBAF as the requirements are very similar. Table 2 shows the target parameters.

Obviously this target is a general purpose facility for CEBAF, useful for many other experiments, including the *Deformation of the* Δ proposed by this collaboration. However, the primary motivation for undertaking the construction of the target is to measure G_{en}.

4 Detectors

4.1 Electron Spectrometer and Detection System

The HMS in Hall C or the HRS in Hall A have the necessary combination of momentum acceptance, resolution, and solid angle for this experiment. Only modest energy resolution on the electron side is necessary as the neutron arm dominates the overall determination of the missing energy. The large vertical acceptance of these spectrometers is an advantage when considering the deflection of the electrons in the target field. For the present experiment, we will use the HMS in the reverse-quad mode, which offers a larger solid angle (10 msr). The tradeoff of horizontal for vertical acceptance is also desirable as it allows to maintain the condition of $\vec{q}$ perpendicular to the target polarization over a larger acceptance.

The detection package will consist of drift chambers for reconstruction of the electron angles and momenta; for particle identification, a gas Cerenkov counter and lead glass shower counters; and plastic scintillator hodoscopes for timing and

to help with muon rejection in the shower counter. The needs of this experiment are well within the capabilities of the standard detection system planned for the CEBAF electron spectrometers. In fact, the low rates we anticipate will not pose a problem to their rate handling capabilities.

4.2 Neutron Detector

Quasielastic scattering events from the neutron will be identified by detecting the recoil neutron in coincidence with the scattered electron. The neutron detector will consist of an array of scintillators which will form a continuous wall. The front of the detector will be covered by a layer of ΔE detectors for the identification of protons. A thin layer of lead (a few mm to 1 cm thick, depending on background conditions) will shield the detector from soft x-rays coming from the target.

The size of the neutron detector is determined by two factors:

1. The solid angle required to match the electron spectrometer solid angle and contain the Fermi-broadened neutron peak corresponding to the quasi-elastic electron peak.

2. The neutron flight path necessary to obtain the required energy resolution to separate the quasielastic recoiling neutron from background events, Δ-excitation in particular.

To determine the required solid angle which will match the electron spectrometer solid angle we performed a Monte Carlo calculation to simulate the quasielastic $d(e,e'n)p$ process. The neutron initial momentum was assumed to follow the nucleon momentum distribution in the deuteron. The spectrometer solid angle was assumed to be 10 msr with a momentum bite acceptance of $\Delta p/p = \pm 5\%$. This results in a detector of size 2.6 m (vertical) by 1.3 m (horizontal). This detector is placed at a distance of 3.4, 3.4, 5.5, 8.0 m from the target, for the Q^2 values of 0.5, 1., 1.5 and 2.0 $(\mathrm{GeV/c})^2$, respectively.

There are three major sources of non-quasielastic, background $(e,e'n)$ events;

1. Coincidence events originating from the nitrogen in the polarized target.

2. Charge exchange reactions (discussed later).

3. Coincidence events originating from the process $e + p \rightarrow e' + \pi + n$.

The first two can be determined by measuring the $N(e,e'n)$ reaction under the same conditions, or by a careful measurement of the nitrogen quasielastic peak (which extends beyond the deuteron peak), and subtracted from the deuteron quasielastic events.

The expected spectra with this set up have been calculated using the Monte Carlo code MCEEP[20]. As input we have used the known deuteron momentum distribution, an experimental spectral function for ^{15}N and ^{4}He, the standard nucleon

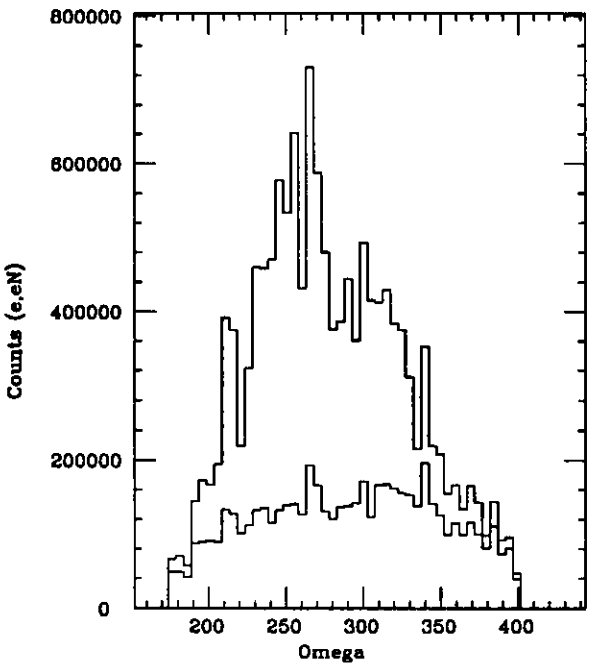

Figure 5: Electron energy loss spectrum for (e,e'n) for ND_3 and ^{15}N-target at Q^2=0.5 $(GeV/c)^2$.

form factors, calculated neutron detector efficiencies and the known acceptance of the HMS. Examples of the resulting spectra (cut on the presence of a recoil neutron and on a value of $\Theta_{pq} \leq 0.1$ rad (which corresponds to a cut in the component of the neutron momentum perpendicular to q) are shown in Figures 5 and 6.

The quasielastic cross section is at worst about equal to that of π production. However, while the neutron detector covers the entire quasi elastic phase space, only part of the phase space of the neutrons originating from π-production processes will be covered by the neutron detector; these neutrons in general correspond to π's of high kinetic energy. The contribution from pion production will be eliminated by measuring the neutron energy via TOF. For the flight paths assumed, and a conservative estimate of the time resolution obtainable (σ = 0.3 ns, see below) we obtain an energy resolution of < 100 MeV. The small contribution to the background from the Δ ensures that this energy resolution will suffice to separate the deuteron quasielastic events from the π-production events.

The neutron detector will be assembled from 1.6 x 0.1 m^2 scintillator bars 10 cm thick; a total thickness of 30 cm will yield about 40% neutron detection efficiency. The University of Virginia has presently operating a similar neutron detector 1.6 x 1.6 m^2, 20 cm thick, with the same scintillating units. With this detector and minimum ionizing particles, a timing resolution of σ=120 ps has been achieved. This detector will be extended to match the size and thickness listed above. At the present time, 48 of the 72 scintillator bars, the ΔE detectors and the associated

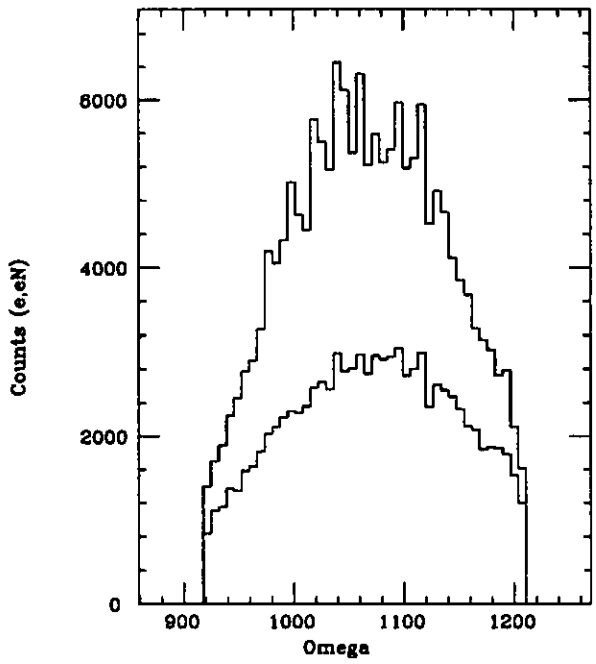

Figure 6: Electron energy loss spectrum for (e,e'n) for ND_3 and ^{15}N-target at Q^2=2.0 $(GeV/c)^2$.

electronics are at hand; the rest will be procured in the course of 1993.

The time resolution aimed for (0.3ns) is achieved more easily if the beam is run at a frequency of 500MHz, rather than 1.5GHz. In this case one could measure the neutron TOF relative to the RF, and use the electron time only to select the appropriate beam bucket. Running at 500MHz would reduce the accuracy needed in the reconstruction of the electron tragectory and TOF in the HMS.

Part of the detector will be covered by a *double* layer of ΔE detectors. This will allow us to check the efficiency in separating protons from neutrons. The analysis of the events from different planes of the E-detector will provide information to the same end.

The shielding in front of the detector needed to remove soft x-rays is expected to be in the thickness range of several mm to 1cm. A thickness of 1–3 mm of lead was sufficient to run at NIKHEF (duty cycle 1%, peak current of 30μA, target thickness of 50mg/cm^2) a successful d(e,e'n) experiment that measured the neutron magnetic form factor by detecting recoil protons and neutrons *simultaneously*, using a similar setup as proposed here [19]. Given the much more favourable conditions (lower luminosity, duty cycle) of the proposed experiment, we expect no difficulties with high single rates or accidental rates.

5 Charge exchange reactions

Not all events identified as a coincidence between an electron and a neutron necessarily correspond to the (e,e'n) process. The reaction (e,e'p), followed by charge exchange (p,n) can produce events of similar signature.

Two types of charge exchange processes occur:

- Charge exchange within the nucleus that produced the (e,e'p) reaction.
- Charge exchange in the rest of the target and the shielding between target and detectors.

The former process can not be distinguished experimentally from (e,e'n). For the special case of the deuteron the contribution can be calculated accurately. A calculation by Arenhövel confirms that the effect is <2% for the asymmetry in our Q^2-range. The (e,e'p) events from ^{15}N followed by a coherent (p,n) final state interaction have the same signature as the ^{15}N(e,e'n) events and are automatically subtracted out when removing the wide nitrogen quasielastic peak from the the narrow deuteron quasielastic peak.

These same arguments are also valid for ^{15}N(e,e'p) followed by a incoherent charge exchange reaction in the ND_3, target walls, superinsulation etc. The e–n coincidence events from the process d(e,e'p) and subsequent (p,n) in the target etc. however have the same signature as the genuine d(e,e'n) events and have to be removed via a calculated correction.

To estimate the contribution of this effect we extrapolate from measured A(p,n) cross sections [11, 12, 13]. We assume the same energy dependence of the zero degree A(p,n) cross section as for basic (p,n) scattering because the dominant reaction process for emerging high energy neutrons is a quasifree interaction in the region of interest (100 - 1000 MeV). Furthermore we employ an A-dependence of $A^{2/3}$ assuming that the reaction is mainly sensitive to the surface. Such an A-dependence describes reasonably well the existing data[11]. With this procedure, we estimate the contribution to the asymmetry assuming a 2cm thick ND_3-target to be <0.24% in our Q^2-range. The contribution is highest at the lowest Q^2-point due to the high ratio of cross sections d(e,e'p)/d(e,e'n). However the contribution is negligible for the present proposal.

This is an advantage over measurements using the recoil polarization of the neutron to determine G_{en}. The heavy shielding in front of the polarimeter represents a very thick target that increases the probability for the process d(e,e'p) + (p,n) to a point where an accurate calculation is needed to correct for the effect. For example, at a proton energy of 800 MeV and a polarimeter shielding of 12 cm Pb, we estimate this process to contribute a false asymmetry of order 5%.

6 Uncertainties in G_{mn}

An accurate knowledge of the magnetic form factor G_{mn} is of particular importance for a determination of G_{en} because the relevant term of the measured asymmetry is proportional to $G_{mn} \cdot G_{en}$. The present accuracy of G_{mn} is not better than 10% due to the systematic uncertainties resulting from the deuteron model required to extract G_{mn} from quasielastic d(e,e') and d(e,e'p) data.

Part of the collaboration is involved in experiments using a method that is not subject to these limitations. These experiments determine G_{mn}via a measurement of the cross section ratio R = d(e,e'n)/d(e,e'p) in quasifree kinematics which is *independent* of the deuteron model used because the initial momentum distribution for proton and neutron are identical. The price one pays is that in such a measurement the absolute neutron detection efficiency of the detector must be known with great precision.

Such an approach was explored for the first time in an experiment at the NIKHEF electron accelerator at Q^2-values of 0.09 and 0.13 $(GeV/c)^2$. The neutron detector was calibrated at the neutron beam facility at PSI in Switzerland. The experiment will produce data with an accuracy of <3% in G_{mn}. These measurements will be extended to cover a Q^2- range of 0.1 - 0.8 $(GeV/c)^2$ using the electron and neutron beams at Mainz and PSI. Thus very precise data for G_{mn} will be available at the time they are needed for the present experiment.

7 Beam current monitoring

The primary current monitor for the experiment will be an ion chamber based on a successful design from LAMPF. It will provide absolute current measurements of several percent accuracy, and relative measurements of the two spin state currents to better than .01% accuracy. The active collection region of the ion chamber is 10 cm long. With a working gas of Helium at atmospheric pressure, the chamber gain will be of order 10^2. A large signal to noise ratio is achieved by using exceedingly high resistivity fused quartz standoffs. Leakage currents less than 100 pA are expected.

In order to avoid significant ion pair recombination due to space charge effects, the beam current density at our operating field of 1 kV/cm must be kept below 1 nA/cm^2. This is achieved in this experiment by placing the ion chamber downstream of the target, at the entrance to the beam dump tunnel, where the multiply scattered beam spot is very large.

The ion chamber is currently under construction by members of the collaboration at CEBAF, and will be installed as a permanent element in the Hall C beamline before the start of physics. The materials used in the construction have been carefully selected to avoid problems with activation and radiation damage. Whenever possible, aluminum has been used in place of stainless steel, and no organic materials will be used in the construction.

8 Low-current operation

For experiments with the polarized target, the CEBAF accelerator should be operated with average beam currents in the range 10nA to 100nA. This could represent a problem, as the instrumentation of the accelerator is designed for a minimal beam current of 1μA. In this section we show how this difficulty can be circumvented.

Low-current operation actually encounters a set of problems:

- The present gun is not able to deliver *simultaneously* low currents and currents in the range of 100μA, thus restricting the flexibility in the choice of beam currents delivered to simultaneous users in different halls.
- The polarized source equipped with a stressed photocathode (delivering 80% polarization) is not suitable for high beam intensity operation (above several μA) due to the small quantum efficiency.
- The accelerator is not instrumented for currents much below 1μA.

These complications are solvable. The solutions for the case of 3 halls running simultaneously will, however, not be implemented at the time we plan to run our experiment.

The solution for running the G_{en}-experiment is a straightforward one:

- Running the experiment in the first 1.5 years where only Hall C is operative makes Hall C the *single user* of the accelerator, and the question of greatly differing beam currents for *simultaneous* users does not arise.
- The G_{en} experiment only requires *low* beam currents ($\leq$ 100nA for the physics running, potentially $\leq 1\mu$A for additional irradiation of the ND_3 target at 1K). The experiment therefore gets all the current needed from the presently available stressed GaAs cathodes (which are used in experiment E143 at SLAC which runs in Fall 1993)
- The monitoring of the beam in the accelerator can be carried out by adding to the low intensity CW-beam spikes of 50–100μs duration and 1μA peak intensity. This scheme again is already implemented at SLAC where the beam monitoring system has the same difficulties with the low intensities required by the polarized target. Such a spike can be produced in the polarized source by adding a further Pockels (or Kerr) cell.

The monitors at CEBAF used for the steering of the beam have time constants of less than 50μs. A spike of $>50\mu$s duration and 1μA intensity can be sampled, and used to control the beam position. The rate of these spikes is expected to be in the $10 - 100\ s^{-1}$ range, contributing an additional *averaged* current of 0.5 – 5 nA. This additional intensity is perfectly acceptable to the polarized target.

During these spikes of high peak intensity, we plan to veto the data acquisition (a loss of duty cycle of less than 1%). We also envisaged using the beam rastering system to steer the beam during the spike to a point 2 mm below the ND_3 target, such that, due to the low target density at that point, the spike would add *nothing at all* to the overall radiation dose received by the target.

9 Compensation for Target Field Effects

When using a polarized target, the holding field deflects all charged particles entering and exiting the target. For the $\vec{d}(\vec{e}, e'n)$ case of interest, the holding field is in the scattering plane, in the direction perpendicular to $\vec{q}$. The field has a component perpendicular to both the incident and scattered electron directions and results in small, yet significant deflections. This deflection of the electrons is minimized by performing the experiment at the highest incident energy (which corresponds to the smallest angle) possible. This at the same time yields a figure of merit close to the maximal one. For the energies and angles listed in Table 1 the maximum deflection for the incident electron in traversing a target field of 1.34 T–m is 4.3°. For the scattered electron the maximum deflection is less than 3.3°.

Unless compensated for, the deflection of the incident and final electrons can be troublesome. When the beam is deflected down, the scattering plane is tilted such that $\vec{q}$ points toward the floor. The angular direction of $\vec{q}$ relative to the laboratory floor, ϕ_q, is given by

$$\sin \phi_q = -\frac{E}{q} \sin \phi_b$$

where ϕ_b is the beam deflection angle. At high energies and small angles a small incident beam deflection is magnified, resulting in a large deflection of $\vec{q}$. For example, at $Q^2 = 0.5$, $\frac{E}{q} = 3.8$ and $\phi_q = 14.5°$. Since the scattered electron is deflected vertically as well, the scattering plane has a significant tilt with respect to the floor. To detect the neutron along $\vec{q}$ at a $Q^2 = 2$, the neutron detector at 8 meters from the target would be 1 meter below the horizontal. Further complications arise since the angle of the spectrometer, θ_s is different from the true scattering angle when the beam is deflected. This difference between θ_e and θ_s is greatest in the forward direction.

CEBAF has designed a chicane[22] in coordination with this collaboration in order to compensate for the effects of the target field. This chicane is designed such as to obtain a *horizontal* incident beam at the center of the polarized target. The gap of the magnet will be large enough (2.5cm and 3.8cm for BE and BZ, respectively) to allow for rastering of the beam. The width of the poles is such that the chicane can be used over a large range of incident energies; also, very small deflections (where the chicane magnets can be used to correct the alignment of the incident beam) are possible without mechanical rearrangement of the chicane. The upstream chicane magnets will be part of the initial complement of equipment in

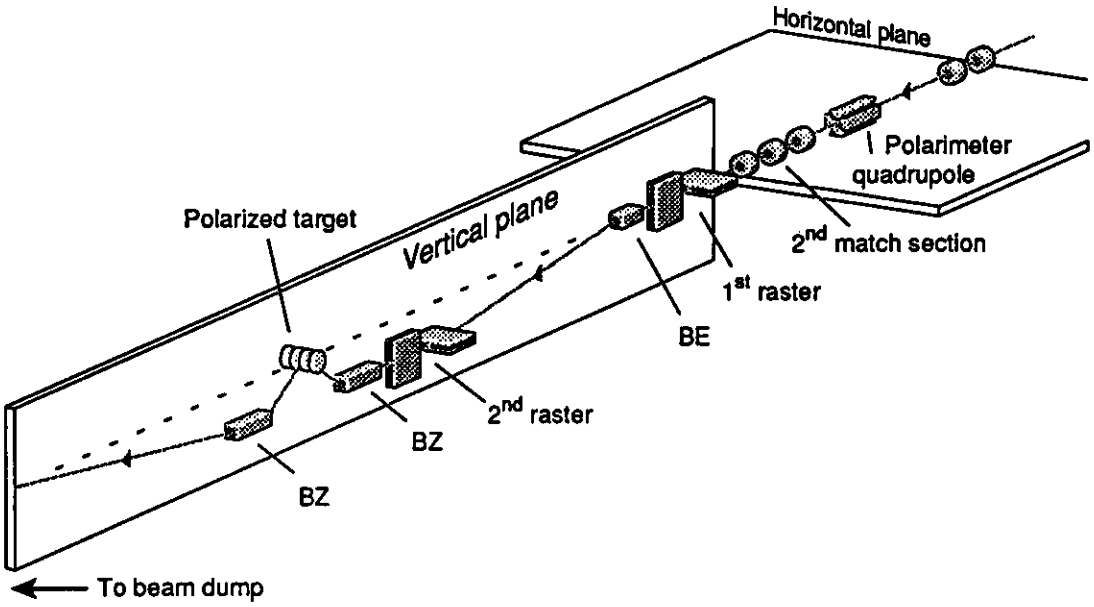

Figure 7: The Hall C chicane. Also indicated is the beam rastering system which will be available when Hall C is ready for beam. Not shown are the beam position monitors and beam current monitors.

Hall C. The downstream chicane will direct the incident beam towards the beam dump.

The chicane is shown schematically in Figure 7. The magnet contracts have been awarded and the magnets should be delivered by September 1993.

10 Electron polarimetry and Møller scattering

To measure the beam polarization the Møller scattering technique will be used. Longitudinally polarized beam electrons will scatter from a target which contains longitudinally polarized atomic electrons. The counting rate for scattered electron depends on whether the spins of the electrons are parallel or anti-parallel. The ratio of the two counting rates is a measure for beam polarization:

$$\frac{d\sigma}{d\Omega} = \frac{d\sigma^{\circ}}{d\Omega} \cdot (1 \pm A_{jk} P_j^B P_k^T) \tag{7}$$

where P_j^B and P_k^T are the beam and target polarization, A_{jk} the asymmetry coef-

ficients. For energies higher than 1 GeV, there are only three non zero asymmetry coefficients $A_{xx} = -1/9$, $A_{yy} = +1/9$ and $A_{zz} = -7/9$ (maximum values).

Background under the Møller peak is dominated by Mott scattering and its radiative tail. To reduce this background the coincidence technique will be used by detecting scattered and recoiling electron in coincidence. The easiest geometry corresponds to detection under 90° CM. A_{zz} there has its maximum and the cross section is (independent of energy)

$$\frac{d\sigma^{\circ}}{d\Omega}(\theta_{CM} = 90°) = 178 \cdot Z \ \frac{\text{mb}}{\text{sr}} \tag{8}$$

For energies between 1 and 6 GeV the corresponding 90° CM angles are in the range 1.8^0 to 0.75^0 in the lab frame.

10.1 Target and polarization measurement

Møller polarimeter targets always consist of thin ferromagnetic foils. Foils have a large density of electrons, ferromagnets are easily polarized.

The classical target set-up consists of a foil magnetized in its plane using two Helmholtz coils. The target is oriented to have a small angle (10-20°) with respect to the beam to get longitudinal polarization. Magnetization of the target is measured with the help of pick-up coils which sense the change of flux upon reversal of the B-field. Precision of this method is limited by systematic errors of this measurement process. This leads to typical uncertainties of target polarization between 2 and 5 %.

The target planned for Hall C will be of a novel design. The target will be magnetized to saturation in a field of 4T *perpendicular* to the foil plane using a superconducting split coil. The target magnetization is monitored with help of a laser beam. This design is more costly but has decisive advantages:

- In principle there is no need to measure the target magnetization as long as magnetic saturation can be assumed. This is certainly true for low beam currents as there depolarization due to target heating can be neglected.
- With the laser monitoring foil magnetization can be observed on-line. Problems with target depolarization can be noticed immediately.
- During experiments only the relative target polarization needs to be measured (due to the saturation). The absolute calibration is known from the literature.
- The measurement is insensitive to errors in geometry as the target is perpendicular to the beam.

The target will consist of a pure iron foil, as iron is the ferromagnet with the best known properties. Maximum target polarization at saturation is 2.216 / 26 = 8.52 %. This value must be temperature corrected as ferromagnetism becomes weaker

with increasing temperature. For iron the magnetization vanishes at $T_{Curie} = 770°$ C. The relation between magnetization and polarization is given by:

$$P = \frac{M_s}{\mu_B} = \frac{2 \cdot (g_l - 1) \cdot M}{g_l \cdot \mu_B} \tag{9}$$

The value of M (the magnetization per unit volume) can either be measured in a separate experiment, or taken with very high precision from the literature. The factor g_l (the contribution of the orbital moment to the magnetization) contains the largest uncertainty and is the only value which cannot be measured by ourselves. Its uncertainty is 0.1%.

The magnetization is monitored with help of the magneto-optical Kerr effect. A polarized laser beam is reflected on the target. If the target is magnetized, the reflected beam has an altered polarization plane. The rotation of the polarization plane linearly depends on the magnetization. The laser probes the magnetization in the first 50 nm only, but it has been shown that surface magnetization is always *smaller* than its bulk value. Thus saturation of the foil in the surface proves that magnetic saturation exists throughout the material. The set-up is shown in fig.8.

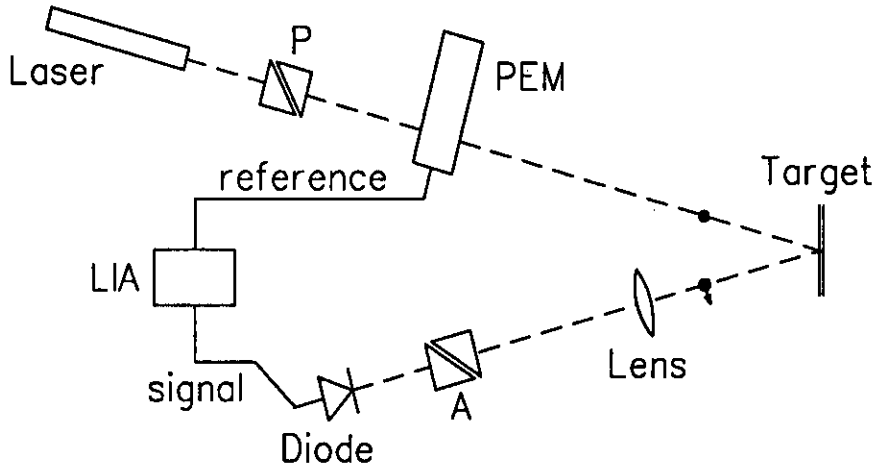

Figure 8: Setup of a Kerr apparatus: P = polarizer(Glan-Thompson), PEM = photoelastic modulator, A = analyzer(Glan-Thompson), LIA = lock-in amplifier

10.2 Quadrupole spectrometer and detectors

The polarimeter is designed to be a *general – purpose* polarimeter for Hall C, operating at energies between 1 and 6 GeV, for a large range of beam currents ($\leq 20\mu A$, higher beam currents can be envisaged at a later time). To achieve this, the beam will be rastered over $\pm$1mm in horizontal and vertical direction, and the target will be continuously moved. At the same time, the layout (see figure 9 is planned to have a *fixed* geometry independent on energy.

These boundary conditions, together with a maximal length of 12 m requires a setup with two quadrupoles. The lower energy Møller electrons (large scattering angle) get focussed by the first quad (which needs only little bending power) in order to pass through the second one, where they are bent away from the beam. The higher energy Møller electrons (at small scattering angles) are only affected by the second quad and make use of its maximal bending power. With the two-quad setup a separation of 50 cm between the beam and the 90^0CM Møller electrons is achievable for all incident beam energies.

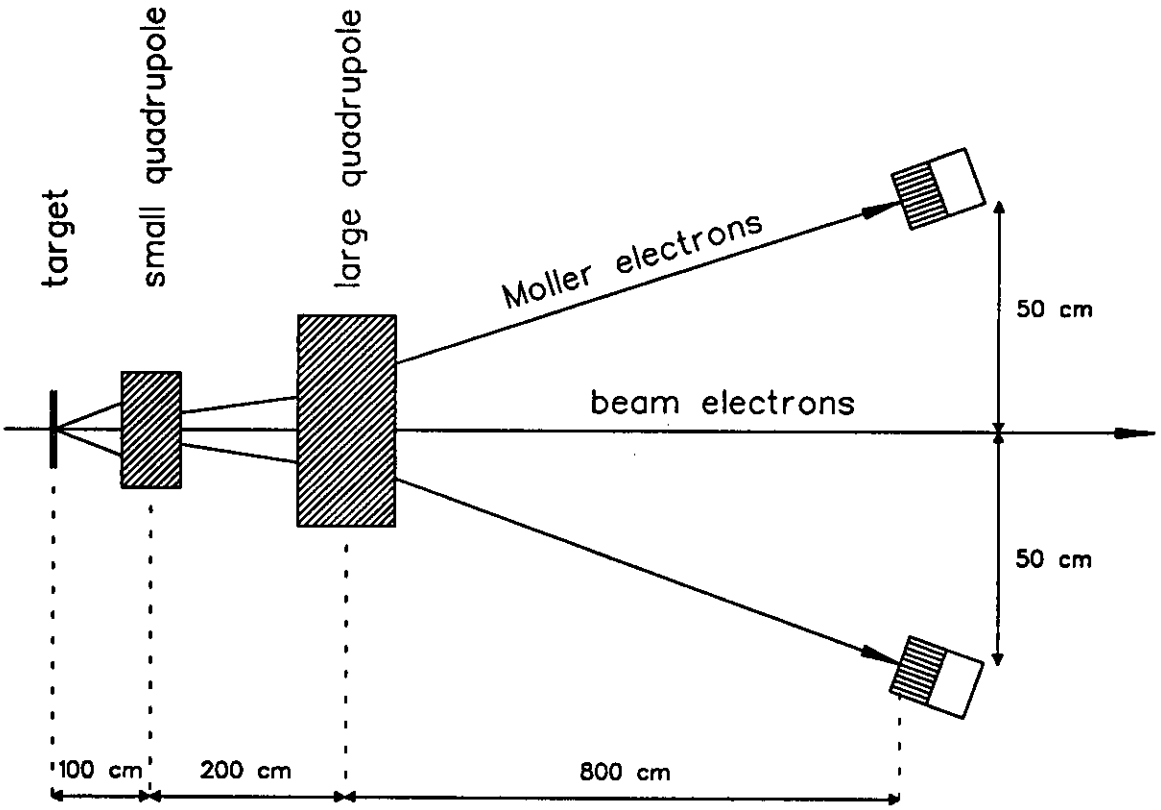

Figure 9: Setup with two quadrupoles which produces a separation of 50 cm between the beam and the detectors with a total length of 12 m.

Two total absorption lead glass shower counters are used as detectors. Energy discrimination and left-right coincidence will ensure identification of a real Møller event. To check the optics and the settings of the quadrupoles, a hodoscope in front of the shower counters gives the exact position information of the Møller pairs. The hodoscope is available during all data taking runs and allows an online check for the quadrupole settings. The setup for the electronics of the two shower counters and the 16 channel hodoscope is shown in fig. 10.

The count rate used in the determination of the polarization is simply given by the coincidence rate between the shower counters, which is counted in a fast scaler. The hodoscope is read out only if a valid shower counter coincidence was detected

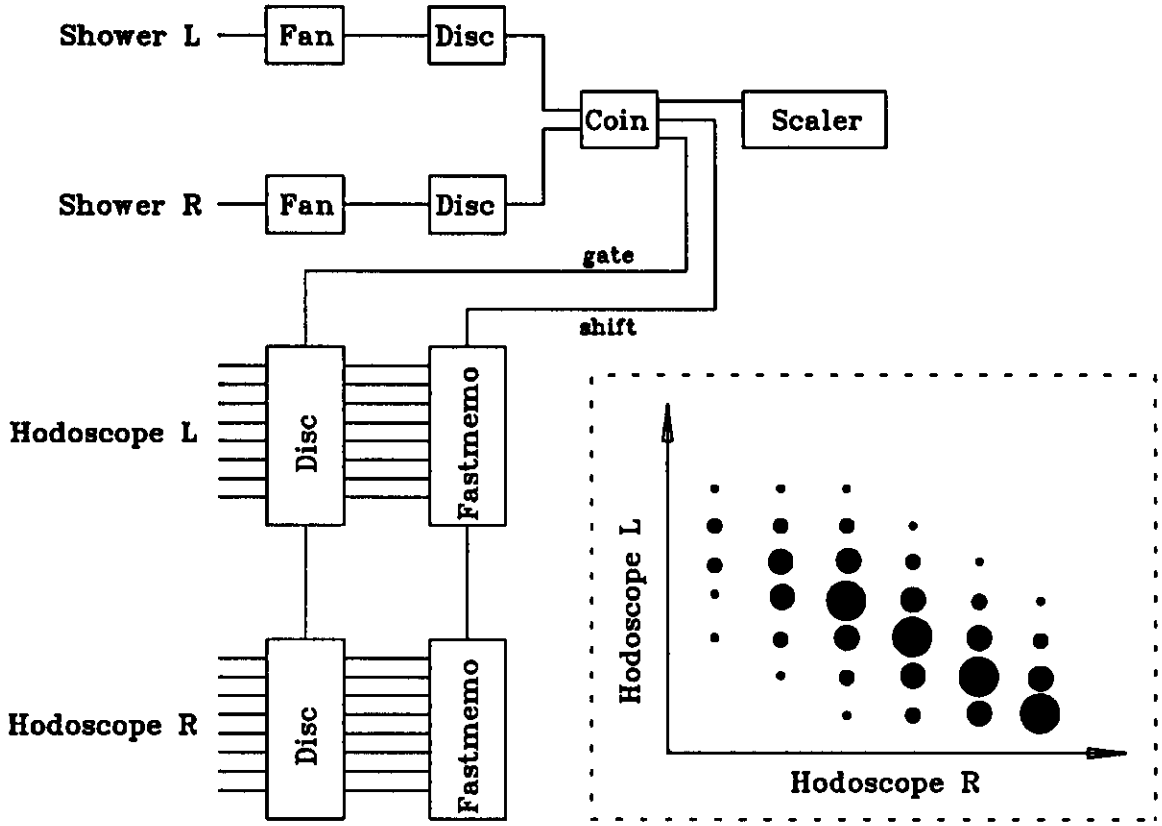

Figure 10: Setup of the electronics for shower counters and hodoscopes, insert: Hodoscope spectrum

and then stacked in two memories which stack 16K events before read out. The hodoscope positions of the Møller pairs produce, if the setup is correctly tuned, the event distribution shown in fig.10 (insert).

With the layout planned (Fe foil thickness $20\mu m$, beam current $100nA$) a determination of the beam polarization to an accuracy of ± 0.01 takes 12 minutes.

The setup to measure the Møller target polarization has been developed and is running in Basel; studies to improve stability are still underway. The split superconductive solenoid has been procured from Oxford instruments and is available. The large quadrupole has been refurbished at CEBAF and is ready for installation by late '93. The optics of the 2-quad system have been studied, and the electronics for the readout of the detectors have been purchased. The mechanism to move the target, additional rastering of the beam by $\pm$ 1 mm (for spreading the heat), collimators, vacuum enclosures and the hodoscope detectors are being worked on.

11 Simultaneous measurement of G_{ep}

The electric form factor of the proton G_{ep} can also be measured during this experiment with a minimum of overhead and additional instrumentation. There are two ways of determining G_{ep} with polarized ammonia targets: measuring the inclusive cross section asymmetry for elastic $e-p$ scattering on the polarized hydrogen nuclei in NH_3, and measuring the asymmetry for electrodisintegration of the deuteron, with detection of the polarized protons in ND_3. Both methods can be used in the present experiment. The former approach is of interest for an accurate determination of G_{ep}, the latter method provides an ideal test of our understanding of the reaction mechanism of the $\vec{d}(\vec{e},e'n)$ reaction used for the determination of G_{en} as the *same* reaction with the same potential complications (FSI, MEC) is used to measure a ***known*** quantity, G_{ep}.

For a precise determination of G_{ep} the easiest way is the measurement of the asymmetry

$$A_{ep}^{el} = \frac{-2\sqrt{\tau(1+\tau)}\tan(\theta_e/2)G_{ep}G_{Mp}}{G_{ep}^2+\tau(1+2(1+\tau)\tan^2(\theta_e/2))G_{Mp}^2}$$

by detecting the electrons scattered elastically from the protons in ammonia. The experimental asymmetry

$$\varepsilon = \frac{N_+ - N_-}{N_+ + N_-} = P_b P_t A_{ep}^{el} f$$

is related to A_{ep}^{el} through the beam and target polarizations P_b and P_t, and the dilution factor f, which is just the ratio of the number of polarizable hydrogen nuclei (N_p) times the unpolarized cross section σ_p to the sum of the number of nuclei of each atomic species in the target material times their respective $e-A$ cross sections $\sigma_{eA} = \int d^2\sigma_A/(dE'd\Omega_e)dE'$, integrated over the experimental width of the elastic peak:

$$f = N_p\sigma_p / \sum N_A\sigma_A. \qquad (10)$$

In the region of energy loss, ν, of the elastically scattered electrons, σ_A is dominated by the quasielastic scattering contribution. For an estimate of the rates, the full magnitude of σ_A can be calculated with the aid of the QFS code of Lightbody and O'Connell. The experimental width of the elastic peak has been estimated from the beam and final electron energy resolutions, spectrometer angular resolution and contributions from energy losses and multiple scattering in the target and electron path. The estimates range from $\delta E' = 14$ MeV at low Q^2 to 17 MeV at high Q^2.

For the input values of $P_b = 0.8$, $P_t = 0.9$, and using the HMS solid angle acceptance of 10.4 msr we have computed the expected counting rates and required time to measure A_{ep}^{el} with 2% statistical precision. The luminosity assumed is the same as that of the G_{en} part of this proposal: 40×10^{33} Hz cm^{-2}. The results are shown in the table 3.

Q^2 $(GeV/c)^2$	A_{ep}^{el}	σ_{ep} nb/sr	σ_{eA} nb/sr	f	Rate *Hz*	Time *hours*
0.5	-13.7%	438	309	0.80	226	0.5
1.0	-14.2%	60	29	0.84	29.2	3.1
1.5	-16.5%	9.7	4.6	0.84	4.8	14.1
2.0	-18.3%	2.2	0.95	0.86	1.1	46

Table 3: Running conditions for possible measurement of proton charge form factor (rate includes quasielastic background)

In this type of measurement, a correction has to be made for the asymmetry (entirely quasielastic) induced by the polarization of the nitrogen. This small systematic effect can be estimated with reasonable accuracy from the shape of the scattered electron spectrum on both sides of the elastic peak. Its magnitude is small because the contribution to this asymmetry comes from the unpaired proton in ^{15}N only, the paired nucleons in this nucleus cannot be polarized. In addition, this asymmetry can actually be computed from the easily measured polarization of ^{15}N and its shell structure, which places the unpaired seventh proton in a $1p_{1/2}$ state, with a net 1/3 probability of being aligned opposite to the ^{15}N spin. Measurements of the ^{15}N polarization in $^{15}NH_3$ indicate that $P_N \cong 20\%$ for $P_H \cong 95\%$, so the expected nitrogen contribution is $-(1/3) \times (1/3) \times 0.2 = -2.2\%$ of the proton asymmetry. The uncertainty in this contribution is less than 10%.

The above estimates show that $\vec{p}(\vec{e}, e)p$ is a highly competitive method for a precision determination of G_{ep}. The corresponding data taking times are actually considerably smaller than the ones discussed in the $p(\vec{e}, e'\vec{p})$ proposal of Perdrisat *et al* (PR89-014).

Of more direct interest to the determination of G_{en} is the option to measure G_{ep} via the $\vec{d}(\vec{e}, e'p)$ reaction. This reaction involves the same complications as the $\vec{d}(\vec{e}, e'n)$ reaction used for the determination of G_{en} and a measurement of the *known* G_{ep} allows a check of our understanding of the reaction mechanism in an ideal way. FSI and MEC influence $\vec{d}(\vec{e}, e'n)$ and $\vec{d}(\vec{e}, e'p)$ in a nearly identical way.

Such a measurement of G_{ep} via $\vec{d}(\vec{e}, e'p)$ is obviously much easier than the measurement of G_{en}: G_{ep} is much larger than G_{en}, and the detection efficiency for protons is close to one. The rate for G_{ep} is 10 – 100 times higher.

The main difficulty involved with the detection of protons is that the strong target magnetic field produces a substantial deflection of the protons. For the integrated field times path length magnitude of 1.34 Tesla-meters table 4 shows the total vertical deflection of the protons at the plastic detector location.

The column labelled Φ_{se} contains the deflections of the scattered electrons that

start in the horizontal plane; Φ_{sp} are the deflections of the corresponding protons that also leave the scattering point horizontally; Φ_{sp}' on the other hand is the deflection angle of the protons associated with electrons that enter the spectrometer at the horizontal plane after being deflected downward, from an upward initial direction. The latter protons would correspond to an electron phase space that is symmetric about the horizontal plane and therefore are the preferred ones for detection. Their deflections are tabulated in the last column. It should be pointed out that these values correspond to protons along the central momentum transfer. For momentum transfers corresponding to the upper or lower limits of the electron spectrometer's horizontal acceptance, the deflections (in parentheses) are smaller or larger, respectively. The worst case is for Q^2=0.5 $(GeV/c)^2$.

Q^2 $(GeV/c)^2$	Φ_{se}	$\vec{P}_p$ GeV/c	Φ_{sp}	Φ'_{sp}	Path *m*	Vertical Deflection *m*
0.50	2.0°	0.760	17.3°	10.4°	3.4	0.62 (0.51 to 0.78)
1.00	2.3°	1.136	11.6°	4.6°	3.4	0.27 (0.19 to 0.34)
1.50	2.8°	1.465	9.0°	2.9°	5.5	0.28 (0.22 to 0.35)
2.00	3.2°	1.773	7.4°	2.1°	8.	0.29 (0.26 to 0.36)

Table 4: Deflection of recoil protons

It is apparent from the above table that, with the exception of the Q^2=0.5 $(GeV/c)^2$ point, the deflection of the proton represents no problem. The neutron detector has large enough acceptance to detect the recoil protons, and the proton data will be obtained simultaneously with the neutron data. If the test of the reaction mechanism needs to be extended to Q^2=0.5 $(GeV/c)^2$, a (very short) run with the neutron detector raised by 60cm could be performed.

The contributions of the polarized protons in nitrogen are somewhat larger than in the case of inclusive measurements, even if $^{15}ND_3$ is used, because the nitrogen polarization is $\simeq 1/2$ of the deuteron, so the correction is $-1/18 = -5.5\%$, a correction that easily can be calculated to the accuracy desired for the check envisaged here. On the other hand this choice of ^{15}N as target material has the very important additional advantage of entirely eliminating the nitrogen polarization contributions to the neutron measurement since G_{en} will be measured with *electron − neutron* coincidence spectra, which obviously contain no proton contamination, except from second order processes, as discussed elsewhere in the proposal.

12 Estimate of Uncertainties

In systems that have a mixture of polarizable and non-polarizable material, such as ammonia, the target asymmetry A_{ed}^V is related to the experimental asymmetry through

$$A_{ed}^V = \frac{\varepsilon}{f p_b P_t}; \qquad (p_b = p_{beam}, \quad P_t = P_d^1), \tag{11}$$

where f is the dilution factor that includes the effect of the unpolarized nuclei (see the discussion around Eq.(10).

The uncertainty δA_{ed}^V can therefore be expressed as

$$\left(\frac{\delta A_{ed}^V}{A_{ed}^V}\right)^2 = \left(\frac{\delta\varepsilon}{\varepsilon}\right)^2 + \left(\frac{\delta p_b}{p_b}\right)^2 + \left(\frac{\delta P_t}{P_t}\right)^2 + \left(\frac{\delta f}{f}\right)^2, \tag{12}$$

which is a valid expansion since these uncertainties are uncorrelated. From $\varepsilon = (N_+ - N_-)/(N_+ + N_-)$, one can obtain the exact expression $\delta\varepsilon = 2\sqrt{N_+ N_-}/(N_+ + N_-)^{\frac{3}{2}}$ which can be approximated as $\delta\varepsilon \cong 1/\sqrt{N}$, for the usual case of small ε (implying $N_+ \cong N_- \cong N/2$). Therefore

$$\left(\frac{\delta A_{ed}^V}{A_{ed}^V}\right)^2 = \frac{1}{(f A_{ed}^V p_b P_t)^2 N} + \left(\frac{\delta p_b}{p_b}\right)^2 + \left(\frac{\delta P_t}{P_t}\right)^2 + \left(\frac{\delta f}{f}\right)^2. \tag{13}$$

It is expected that at CEBAF the beam polarization will be measured with an accuracy of better than 4%, as it has been done at other laboratories[11]. We expect the situation to improve such that we have used 2% in our estimates. The target polarization has been determined to $\pm 5\%$ in current designs, but, based on CERN experience, we expect to ultimately do better.

The magnitude of δA_{ed}^V is determined by the requirement that it should allow to discriminate among the various models for G_{en}, and it has to be consistent with the lower limits imposed by the uncertainties δp_b, δP_t, and δf. Moreover, it should not represent an unreasonably large number of counts.

From Figure 12 it can be seen that to distinguish, for example, between the Galster parametrization and the Gari-Krümpelmann (G-K) model in the kinematic region of interest, δA_{ed}^V has to be of the order of $\sim 8 \times 10^{-3}$ at the low Q^2 points, to ~ 0.04 on the high momentum transfer side, for a four standard deviation (or better) separation between models. Taking as reference the Galster model, Table 5 illustrates the magnitude of the expected uncertainties in the asymmetry A_{ed}^V, the experimental asymmetry ε and the number of counts needed for the desired level of precision. In this table, the values of N were computed using the following additional assumptions: $p_b = 0.8 \pm 2\%$, $P_t = 0.40 \pm 5\%$, uncertainty in $f = 3\%$.

These values of N have been calculated using the expression

$$N = \frac{1}{(p_b P_t A_{ed}^V f \delta\varepsilon/\varepsilon)^2}. \tag{14}$$

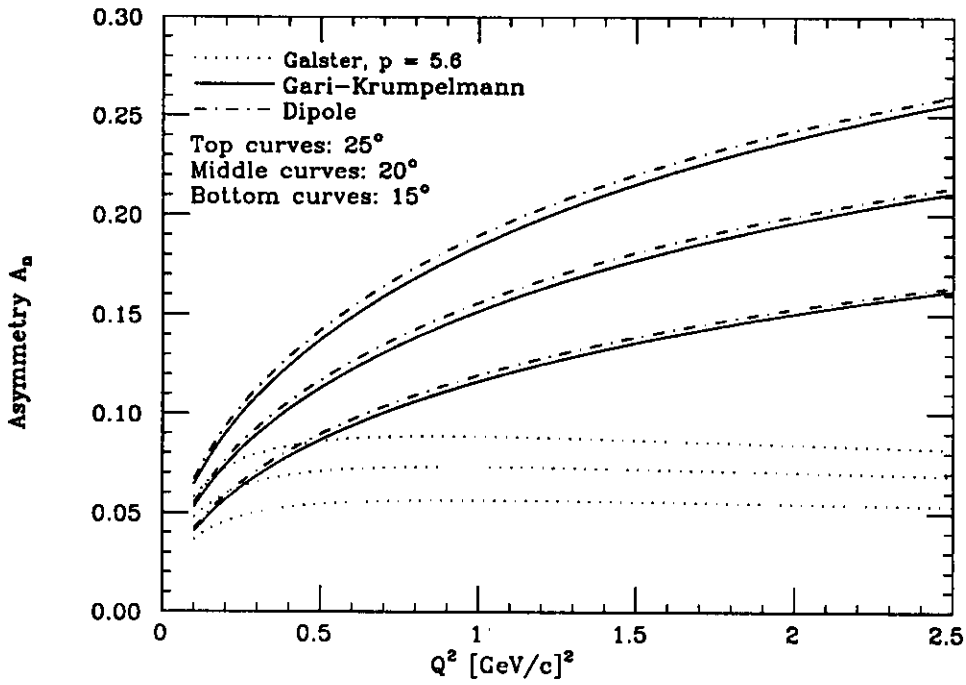

Figure 11: A_n as a function of Q^2 for three models and three angles.

Q^2 $(GeV/c)^2$	θ_e	$\delta A_{ed}^V / A_{ed}^V$	$\delta\varepsilon/\varepsilon$	N	f
0.5	15°	7.0%	4.8%	3.96×10^6	0.61
1.0	15.6°	11.3%	10.0%	1.2×10^6	0.48
1.5	20°	14.2%	13.2%	5.7×10^5	0.43
2.0	24°	19.3%	18.6%	2×10^5	0.46

Table 5: Counts, dilution factors and expected uncertainties

We note that the minimum uncertainty in A_{ed}^V is restricted by the combined uncertainties in p_b, P_t, and f which in the present case amount to $\sim 6\%$.

To obtain G_{en} from the asymmetry, we have to solve the expression for $A_n = A_{ed}^V/\gamma$ (Equation (5)) for the ratio G_{en}/G_{mn}. Since the different models predict that as Q^2 increases, this ratio approaches and even exceeds 1 ($G_{en} = G_{mn}$ at $Q^2 = 4m_n^2$ $(GeV/c)^2$ in the dipole and G-K models), it is inaccurate to neglect the term $(G_{en}/G_{mn})^2$ in the Q^2 range of the present proposal. The result is that we have a quadratic equation for G_{en} that can be written as

$$\left(\frac{G_{en}}{G_{mn}}\right)^2 + \frac{\gamma f(\tau,\theta_e)}{A_{ed}^V}\left(\frac{G_{en}}{G_{mn}}\right) + g(\tau,\theta_e) = 0, \tag{15}$$

where $f(\tau,\theta_e) = 2\sqrt{\tau(1+\tau)}\tan(\theta_e/2)$, and $g(\tau,\theta_e) = \tau(1+2(1+\tau)\tan^2(\theta_e/2))$. The solutions are

$$G_{en} = \frac{-f\gamma G_{mn}}{2A_{ed}^V}\left(1 \pm \sqrt{1 - 4g\left(\frac{A_{ed}^V}{\gamma f}\right)^2}\right). \tag{16}$$

By substituting in this expression the asymmetry predicted by a given model, it is seen that the negative root reproduces G_{en}. Therefore we can write

$$G_{en} = C(1-R); \quad C = \frac{-\gamma f G_{mn}}{2A_{ed}^V}, \quad R = \sqrt{1 - 4g\left(\frac{A_{ed}^V}{\gamma f}\right)^2}. \tag{17}$$

The purpose of this exercise is to obtain an expression for δG_{en}, based on the usual expansion for the uncertainties

$$\delta^2 G_{en} = \left(\frac{\partial G_{en}}{\partial G_{mn}}\right)^2 \delta^2 G_{mn} + \left(\frac{\partial G_{en}}{\partial A_{ed}^V}\right)^2 \delta^2 A_{ed}^v, \tag{18}$$

where the uncertainties $\delta\tau, \delta\theta_e$ and $\delta\gamma$ have been neglected given their very small relative magnitudes.

After the appropriate substitutions are made, we find that

$$\left(\frac{\delta G_{en}}{G_{en}}\right)^2 = \left(\frac{\delta G_{mn}}{G_{mn}}\right)^2 + \left(\frac{\delta A_{ed}^V}{A_{ed}^V}\right)^2 C^2\left(1 - \frac{1}{R}\right)^2 \frac{1}{G_{en}^2}. \tag{19}$$

This equation contains the effects of both the uncertainty in G_{mn} as well as the propagation of the uncertainty in the asymmetry.

Table 6 shows that for the δA_{ed}^V considered earlier, there is a significant effect on G_{en}. The uncertainty in G_{mn} was taken to be 5%, combining our present knowledge of this quantity at the Q^2 values of this proposal, with the improved precision for $Q^2 \leq 1$ (GeV/c)^2 expected from the ongoing measurements of G_{mn} the Basel group is performing at Mainz.

We note that in the estimates given above we have taken care of the nonlinear relationship between the asymmetry and G_{en}(see Equation 5). This nonlinearity results from the fact that for small values of G_{en}, A is proportional to G_{en}, while for very large values and large momentum transfer A depends on G_{en}^{-1}. There obviously is a range where A does not at all depend on G_{en}! This however does not imply that a measurement of A is not useful; one simply has to analyse the data in a different way. The numerator of equation 5 always depends linearly on G_{en}. One therefore can determine G_{en} directly from Δ, and not from $A=\Delta/\Sigma$. This requires the knowledge of the detector efficiency, which can be deduced from a short cross

Q^2 $(\mathrm{GeV/c})^2$	θ_e	$\delta A_{ed}^V / A_{ed}^V$	$\delta G_{en} / G_{en}^{Galster}$
0.5	15°	7.0%	8.9%
1.0	15.6°	11.3%	13.7%
1.5	20°	14.2%	16.8%
2.0	24°	19.3%	22.3%

Table 6: Expected uncertainties in G_{en}

section measurement under kinematics where the cross section is dominated by G_{mn}. For the case where the data would correspond to a G_{en} closer to the parametrization of Gari-Krumpelman (where at large momentum transfer the blow-up factor becomes of order 2), one therefore would switch to this strategy, and measure the efficiency in a short run (without need for polarization) at larger scattering angles and the same momentum transfer. The resulting relative error of G_{en} for this case would be smaller than shown in figure 12, due to the larger value of Δ.

13 Count Rates and Beam Time Request

On the basis of the estimated numbers of counts presented in the previous section, we have computed the required counting times, displayed in the table below. We have used a Monte Carlo code [20] to calculate the rates, averaging over the experimental acceptances such that the rate can be given by the following expression,

$$R = \frac{\eta}{f} \mathcal{L} \int \frac{d^3\sigma}{d\Omega_e dE' d\Omega_n} d\Omega_e dE' d\Omega_n. \tag{20}$$

The additional factors in R are:

- $\Delta\Omega_e = 10.4$ [msr], for the Hall C High Momentum Spectrometer.
- $\Delta\Omega_n$ corresponding to a 2.6 m by 1.3 m neutron detector placed at 8 m or less from the target.
- $\Delta E'$ corresponding to about $\pm 5\%$ of the central momentum of the electron spectrometer.
- $\mathcal{L}$ (luminosity) $= 4 \times 10^{34}$, for a 40 nA current, equivalent to 2.5×10^{11} electrons/s, and a target density of $2.8 \times 10^{23} [\mathrm{cm}^{-2}]$ polarizable neutrons for a 2.5 cm long target.
- $\eta \geq 30\%$, the neutron detector efficiency (30% at $Q^2 \geq 1.5 \mathrm{GeV/c}^2$).

Table 13 gives the number of counts, rates and times for each Q^2; the rates have been calculated after averaging over the detector acceptances.

Q^2 $(GeV/c)^2$	N $\times 10^5$	R Hz	t hours
0.5	39.6	11.9	92.5
1.0	12.2	3.43	99.0
1.5	5.7	0.67	235.2
2.0	2.0	0.142	400.0

Table 7: Rates and Running Times

In Figure 12 we show the resulting error bars we expect. They have been calculated for the Galster parametrizations.

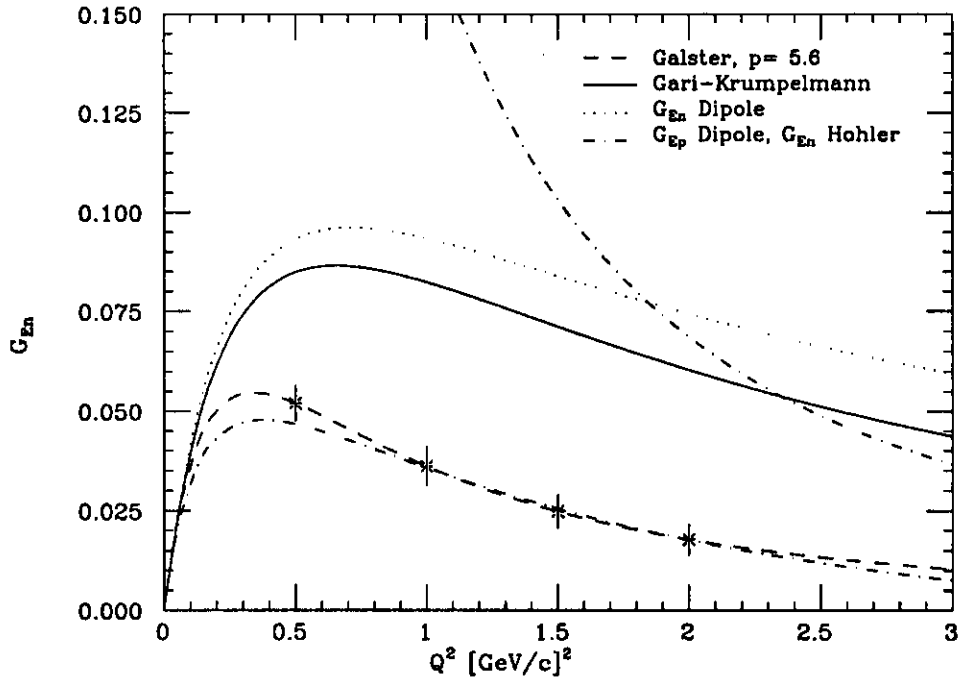

Figure 12: Expected data for G_{en} as a function of Q^2.

In addition, we plan to take measurements on NH_3 targets, to measure the dilution factor and to correct for backgrounds and systematic effects. The measurements on a nitrogen target will be used to extract the backgrounds from the total quasielas-

Data taking	825 hours
NH_3 runs	60 hours
$\vec{e}$ Polarimetry	115 hours
Material Annealing	120 hours
Angle Changes	120 hours
Contingency	200 hours
Total	1440 hours

Table 8: Summary of request

tic peaks, determining in this way the ratio $\beta = N_N/N_{ND_3}$ discussed earlier, in a model independent way.

Considerable time will be spent in beam polarization studies. The disruptive Möller scattering technique does not allow data taking during polarization monitoring. To determine the beam polarization to 3% over long periods will require many short measurements.

An additional entry details the contingency we add to allow for unforeseen difficulties, additional calibrations, etc.

14 Committment of collaboration

Approximately four years ago a decision was made to develop a new laboratory at Virginia to pursue research and development of polarized targets. There were two major goals of this laboratory: 1) to construct high polarization proton and neutron targets suitable for use at CEBAF and other electron facilities; 2) to investigate and develop possible improvement in the existing targets.

The first goal has been accomplished with the procurement and successful operation of an entire system suitable for use in Halls A and C, and with modifications in Hall B. The system consist of the following major components.

- A cryostat containing a 5 Tesla superconducting magnet.
- A series of high capacity root pumps.
- A vertical ^{4}He refrigerator — with operation below 1 K with 1.5 watts cooling power.
- A 140 GHz microwave system.
- An NMR system with variable frequency operation up to 250 MHz.

- A facility for the production of solid state targets - in particular NH_3 and ND_3.

Research has continued in parallel on investigation of other materials and the optimum dose and means of irradiation of the samples. Irradiation of the ammonia samples has taken place at the electron linear accelerator at Saskatchewan and recently at CEBAF. The technique at CEBAF required stopping the 5 MeV injector beam in a tungsten target to generate an intense source of x-rays incident upon the ammonia samples. This was quite successful and we plan to continue this work. We will receive this summer another cryostat and magnet that will be a general purpose research device. The magnet is a superconducting solenoid capable of fields up to 9 Tesla. The central refrigerator is interchangeable, capable of operation with either He evaporation units or a dilution refrigerator. This will allow us to continue our investigation of the optimization of material polarization with variable field and temperature. One of the eventual goals is the construction of a frozen spin system operating at lower temperature and reduced magnetic field.

The cost of procured equipment now totals $1.36M. Basel (Schweizerischer Nationalfonds and the University) and UVA (Higher Education Equipment Trust Fund, Commonwealth of Virginia, the Commonwealth Center and the University) have contributed $1.11M. CEBAF has contributed $253K for the acquisition of the magnet and cryostat.

The manpower effort that has gone into the project is approximately 14 FTE, which includes senior physicists, research associates and technicians, but not students. The Commonwealth Center for Nuclear and High Energy Physics provided salary support for sixty percent of this work while the rest came from the continuing Department of Energy grant at Virginia.

In March 1993 the major components were shipped to SLAC. The target will be installed in end station A for operation in experiment E–143, a precision measurement of the spin structure functions, g_1 and g_2, of the proton and neutron. The experiment is scheduled to run in the Fall of 1993.

The Universities of Basel and Virginia have been developing an improved method of electron beam polarimetry. The new technique involves magnetizing the iron foil perpendicular to the foil plane with a large field (4 Tesla). The target magnetization is continually monitored by a polarized laser beam.

The majority of the system has been procured with funds provided by the University of Basel, and is presently being tested at Basel. The total funds contributed at this time toward equipment for the polarimeter amount to $146K. In addition CEBAF has refurbished the large quadrupole necessary for separation of the Möller electrons. The items that remain to be built are the scattering chamber, the vacuum transport tubes for the beam and the detectors.

Because of the deflection of the incident beam by the high field at the target, it is necessary to install a magnetic chicane upstream of the target. CEBAF has ordered the necessary magnets and power supplies, and is now working on the final design of the beam rastering system.

The work on the large neutron detector was started about four years ago. The very early start was motivated by the possibility of using a smaller version in a series of experiments at the LEGS facility at Brookhaven. A system approximately 50% of the size needed at CEBAF has been in operation at Brookhaven for the last two years. The primary components of the detector are scintillation paddles, scintillator bars (10 cm by 10 cm by 1.6 meters), photomultiplier tubes, and all the associated electronics. The detector will be returned to Virginia this year and we will increase the number of elements. We will purchase an additional 32 scintillator bars and associated electronics.

When completed the detector equipment cost will be approximately $326K. The funds have been provided by the groups from UVA and Basel.

The effort of many scientists and the expenditure of considerable funds have put us in a position to carry out the G_{en} measurement at the earliest time consistent with CEBAF's schedule. All of the items will be built and tested by the end of 1993 and we will be ready to carry out the experiment in the middle of 1994.

With the present proposal we request full approval to run this experiment early in the experimental program of Hall C.

References

[1] A. Amroun *et al.*, Nucl. Phys. **A510** (1990) 740.

[2] Norman Dombey, Rev. Mod. Phys **41** (1969) 236.

[3] T.W. Donnelly and A.S. Raskin, Ann. Phys. (New York) **169** (1986) 247.

[4] T.W. Donnelly and A.S. Raskin, Ann.Phys. (New York) **191**(1989) 81.

[5] R.G. Arnold, C.E. Carlson and F. Gross, Phys. Rev. **C23** (1981) 363.

[6] H. Arenhövel, W. Leidemann and E.L. Tomusiak, Z. Phys. **A331** (1988) 123.

[7] S. Galster et al. Nucl. Phys. **B32** (1971) 221.

[8] M. Gari and W. Krümpelmann, Z. Phys. **A322** (1985) 689, Phys. Lett. **B173** (1986) 10.

[9] G. R. Court and W. G. Heyes, NIM **A243** (1986) 37 - 40, G. R. Court, W. G. Heyes, W. Meyer, and W. Thiel, in Proceedings of the Fourth International Workshop on Polarized Target Materials and Techniques, Bonn, W. Meyer, Editor, 1984.

[10] C. Y. Cheung and R. M. Woloshyn, Phys. Lett. **B127** (1983) 147.

[11] A.M.Kalend, B.D.Anderson, A.R.Baldwin, R.Madey, J.W.Watson, C.C.Chang, H.D.Holmgren, R.W.Koontz, J.R.Wu, and H.Macher. *Phys. Rev.*, C28:105, 1983.

[12] Th. Fischer et al. *Nucl. Instrum. and Methods*, 156:199, 1978.

[13] R. Hess et al. *PSI Proposal R 87-09.0*, 1987.

[14] W. de Boer, J. Low Temp. Phys., 22, 185 (1976)

[15] R. Fernow, Nucl. Instr. and Meth., 148, 311 (1978)

[16] D.G. Crabb, Proc. 9th Int. Symp. on High Energy Spin Physics, Bonn 1990,Eds. Altoff and W. Meyer, Vol. 2, p. 289.

[17] W. Meyer et al. Nucl. Instr. and Meth., 204, 59 (1982)

[18] R. Dostart et al. Proc. 4th Int. Workshop on Polarized Target Materials and Techniques, Bad Honnef, ed. W.Meyer, p. 33, 1984.

[19] J. Jourdan et al., priv. com.

[20] P.E. Ulmer, Monte Carlo for Electr-Nuclear Coincidence Experiments, CEBAF int. Report

[21] D. Crabb, to be publ. in Proc. Int. Symp. High En. Spin Phys., Nagoya, 1992

[22] Chen Yan, R. Carlini, CEBAF int. report CEBAF-R-92-004, 1992